

A NEW PROBE OF LINE-OF-SIGHT MAGNETIC FIELD TANGLING

S. E. CLARK^{1,*}

¹*Institute for Advanced Study, 1 Einstein Drive, Princeton, NJ 08540*

ABSTRACT

The Galactic neutral hydrogen (HI) sky at high Galactic latitudes is suffused with linear structure. Particularly prominent in narrow spectral intervals, these linear HI features are well aligned with the plane-of-sky magnetic field orientation as measured with optical starlight polarization and polarized thermal dust emission. We analyze the coherence of the orientation of these features with respect to line-of-sight velocity, and propose a new metric to quantify this HI coherence. We show that HI coherence is linearly correlated with the polarization fraction of 353 GHz dust emission. HI coherence constitutes a novel method for measuring the degree of magnetic field tangling along the line of sight in the diffuse interstellar medium. We propose applications of this property for HI-based models of the polarized dust emission in diffuse regions, and for studies of frequency decorrelation in the polarized dust foreground to the cosmic microwave background (CMB).

Keywords: cosmic background radiation — ISM: magnetic fields — ISM: structure — methods: analytical — polarization — radio lines: ISM

arXiv:1802.00011v2 [astro-ph.GA] 16 Apr 2018

1. INTRODUCTION

Magnetic fields are notoriously difficult to measure in the interstellar medium (ISM). Observational tracers of magnetic fields include starlight polarization, polarized thermal dust emission, the Zeeman effect, Faraday rotation of linear polarization, and synchrotron emission (e.g., Ferrière 2001). Each of these probes different components of the magnetic field vector, in different phases of the ISM, making a complete description of the magnetic field structure in any region a formidable challenge. Consequently, many questions remain about the structure of the Galactic magnetic field (e.g. Beck et al. 1996; Haverkorn 2015), although significant progress has been made recently by simultaneously constraining multiple components of the field (e.g. Jaffe et al. 2010; Jansson & Farrar 2012).

Recently it was shown that the diffuse neutral hydrogen (HI) throughout the high Galactic latitude sky is populated by thin, linear features, sometimes referred to as HI fibers (Clark et al. 2014). These linear HI structures are extremely well aligned with the plane-of-sky magnetic field as probed by both starlight polarization (Clark et al. 2014) and polarized dust emission (Clark et al. 2015; Kalberla et al. 2016). The structure of the diffuse neutral ISM is deeply coupled to the ambient magnetic field, and the morphology of HI can be used to study magnetism in diffuse environments.

Several specific applications of this phenomenon for measuring interstellar magnetic fields have been proposed. In regions dominated by a strong mean magnetic field, HI orientation can be used to measure the magnetic field strength via a modified Chandrasekhar-Fermi method (Chandrasekhar & Fermi 1953), as demonstrated with observations of linear structures in HI absorption (Clark et al. 2014). At high Galactic latitudes, HI orientation can be used to constrain the polarized dust foreground to cosmology experiments (Clark et al. 2015). These insights have been used to construct models of the Galactic polarized dust emission based in part on the orientation of linear HI structures (Ghosh et al. 2017). In this Letter, we demonstrate a new use of HI morphology and velocity structure: to trace the degree of interstellar magnetic field tangling along the line of sight.

Measuring the degree of magnetic disorder is of interest both for our understanding of the diffuse ISM and for the search for inflationary gravitational wave B -mode polarization in the cosmic microwave background (CMB). These B -modes, if detected, would be definitive evidence for inflation (Seljak & Zaldarriaga 1997), but are obscured by partially polarized thermal emission from magnetically aligned dust grains in the ISM

(Flauger et al. 2014; BICEP2 & Planck Collaborations 2015). Current foreground subtraction techniques rely on measuring the polarized dust signal toward the peak of the dust spectral energy distribution (SED), and extrapolating its contribution to the target frequency. Polarized dust emission is an integral quantity: the vector sum of polarized intensity from magnetically aligned dust grains along the line of sight. Line-of-sight variation in the magnetic field orientation and dust emission properties thus gives rise to “frequency decorrelation,” wherein the polarized sky at one frequency is not simply a scaled version of the polarized sky at another frequency. Observational constraints on this effect are still being refined, after initial measurements of significant decorrelation in the *Planck* data between 353 GHz and 217 GHz (Planck Collaboration L 2017) were found to not be statistically meaningful (Sheehy & Slosar 2018; Planck Collaboration LIV 2018). Frequency decorrelation must be present at some level, and incorrect assumptions about the frequency dependence of polarized foregrounds can upwardly bias measurements of the tensor-to-scalar ratio. In this Letter we demonstrate a novel estimator of one of the primary physical causes of frequency decorrelation: differently oriented magnetic fields along the line of sight. We propose a new use of HI morphology for modeling polarized dust foregrounds.

2. METHODS

We use HI data from the Galactic Arecibo L-Band Feed Array Survey (GALFA-HI; Peek et al. 2018), a survey of the 21-cm HI line over the Arecibo sky (decl. $-1^{\circ}17'$ to $+37^{\circ}57'$ across all R.A.) at $4'$ spatial resolution and 0.18 km s^{-1} spectral resolution, with 150 mK median rms noise per 1 km s^{-1} channel. We analyze a $\sim 3417 \text{ deg}^2$ region of GALFA-HI data at high Galactic latitudes, avoiding the edges of the Arecibo declination range where telescope scan artifacts are more prominent. We quantify the orientation of linear structures in the GALFA-HI survey using the Rolling Hough Transform (RHT; Clark et al. 2014). The RHT is a machine vision algorithm that measures linear power as a function of orientation angle on the plane of the sky. Given image-plane data $I(x, y)$ the RHT returns linear intensity $R(\theta, x, y)$. We run the RHT over the entire GALFA-HI sky, on velocity channels of width $\delta v = 3 \text{ km s}^{-1}$, from $v_{l_{sr}} = -36.4 \text{ km s}^{-1}$ to $v_{l_{sr}} = +36.4 \text{ km s}^{-1}$ (where $v_{l_{sr}}$ is the velocity with respect to the local standard of rest). The RHT parameters are the same as those used in Clark et al. (2015). We also make use of a stray radiation-corrected column density map created from the velocity-integrated HI brightness temperature under the optically thin assumption. The HI data,

including the column density map, and the RHT data product are all publicly available as part of the GALFA-HI Data Release 2 (Peek et al. 2018).

For each velocity channel, we calculate the point estimate of the HI orientation. That is, we define

$$Q_{RHT}(x, y, v) = \int \cos(2\theta) \cdot R(\theta, x, y, v) d\theta \quad (1)$$

$$U_{RHT}(x, y, v) = \int \sin(2\theta) \cdot R(\theta, x, y, v) d\theta, \quad (2)$$

such that each pixel in each velocity channel has a value

$$\theta_{RHT} = \frac{1}{2} \arctan \frac{U_{RHT}}{Q_{RHT}}, \quad (3)$$

measuring the local orientation of linear HI features. We mask any pixels that have zero RHT-measured linear intensity, i.e., any (x_0, y_0) where $\int R(\theta, x_0, y_0) d\theta = 0$.

We define a metric for the degree of coherence of HI orientation as a function of velocity. This parameter, which we call t_{HI} , is constructed analogously to the dust polarization fraction p , and similarly has a theoretical range of $[0, 1]$. We define new Stokes-like parameters using the orientation of HI weighted by the local HI intensity, and integrate over the line-of-sight velocity (v_{lsr}). That is,

$$Q_{HI} = \int I_v \cos(2\theta_{RHT}(v)) dv \quad (4)$$

$$U_{HI} = \int I_v \sin(2\theta_{RHT}(v)) dv, \quad (5)$$

where I_v is the HI intensity in a given velocity channel.

Our measure of how much the orientation of HI varies along the line of sight is then

$$t_{HI} = (Q_{HI}^2 + U_{HI}^2)^{1/2} / I_{HI}, \quad (6)$$

where I_{HI} represents the total HI intensity integrated over the same velocity range. When θ_{RHT} varies significantly along the line of sight, t_{HI} will have a lower value. By contrast, when the orientation of HI is fairly uniform in velocity space, or when only a single linear HI feature dominates the HI emission along the line of sight, the magnitude of t_{HI} will be higher. We refer to t_{HI} as ‘‘HI coherence’’ to evoke this behavior.

We compare HI coherence with the measured fractional polarization of the *Planck* 353 GHz emission. This is defined from the linear Stokes parameters as

$$p_{353} = P_{353} / I_{353}. \quad (7)$$

The polarized intensity P_{353} is naively equal to $(Q_{353}^2 + U_{353}^2)^{1/2}$, and so Equation 6 is defined in analogy to Equation 7. In practice, however, the quadratic dependence on Q and U makes P_{353} a noise-biased quantity. To mitigate this we compute the debiased point estimate \hat{P}_{353} using the Plaszczyński et al. (2014) modified asymptotic estimator (see also Montier et al. 2015a,b). \hat{P}_{353} is computed from the publicly available *Planck* 353 GHz Stokes parameters and covariance matrices (Planck Collaboration VIII 2016). For clarity here we indicate debiased quantities with a hat, but p_{353} is henceforth always constructed from the debiased \hat{P}_{353} .

The values t_{HI} and p_{353} are compared at an angular resolution of $90'$, computed by convolving Q_{RHT} , U_{RHT} , Q_{353} , and U_{353} with a Gaussian kernel with FWHM= $90'$. We also smooth the 353 GHz noise covariance matrix prior to computing p_{353} (see Appendix A of Planck Collaboration XIX 2015). Any pixels that have a signal-to-noise ratio (SNR) < 2 on p_{353} at the 90% confidence level are masked from the analysis. The region of sky analyzed in Section 3 has a median $p_{353}/\sigma_p \sim 11$ at $90'$, where σ_p is the standard deviation of the Plaszczyński et al. (2014) estimator.

3. RESULTS

We find that t_{HI} and p_{353} are correlated across this region of high Galactic latitude sky. Figure 1 shows a heatmap of both quantities at $90'$ resolution on the plane of the sky. In the region shown, the GALFA-HI $|v_{lsr}| \leq 90$ km s $^{-1}$ column density map smoothed to an angular resolution FWHM= $90'$ has a maximum value of $N_{HI} \sim 9.3 \times 10^{20}$ cm $^{-2}$, and a median value of $N_{HI} \sim 2.4 \times 10^{20}$ cm $^{-2}$. At these low column densities, the scatter in p_{353} for a given N_{HI} is large, and p_{353} is not strongly dependent on N_{HI} (Planck Collaboration XIX 2015).

The range of values of t_{HI} in the region analyzed is larger than that of p_{353} . Although t_{HI} is not a physical model of p_{353} , the larger values of t_{HI} can be understood phenomenologically. HI coherence quantifies the velocity-space alignment of linear HI structures *on the plane of the sky*. The true degree of line-of-sight magnetic field tangling, however, depends on the three-dimensional magnetic field orientation. Simple models for polarized dust emission compute linear Stokes parameters that are proportional to a density-weighted integral of the local magnetic field orientation, so that

$$Q_{dust} \propto \int \rho \cos(2\theta) \cos^2\gamma ds \quad (8)$$

$$U_{dust} \propto \int \rho \sin(2\theta) \cos^2\gamma ds, \quad (9)$$

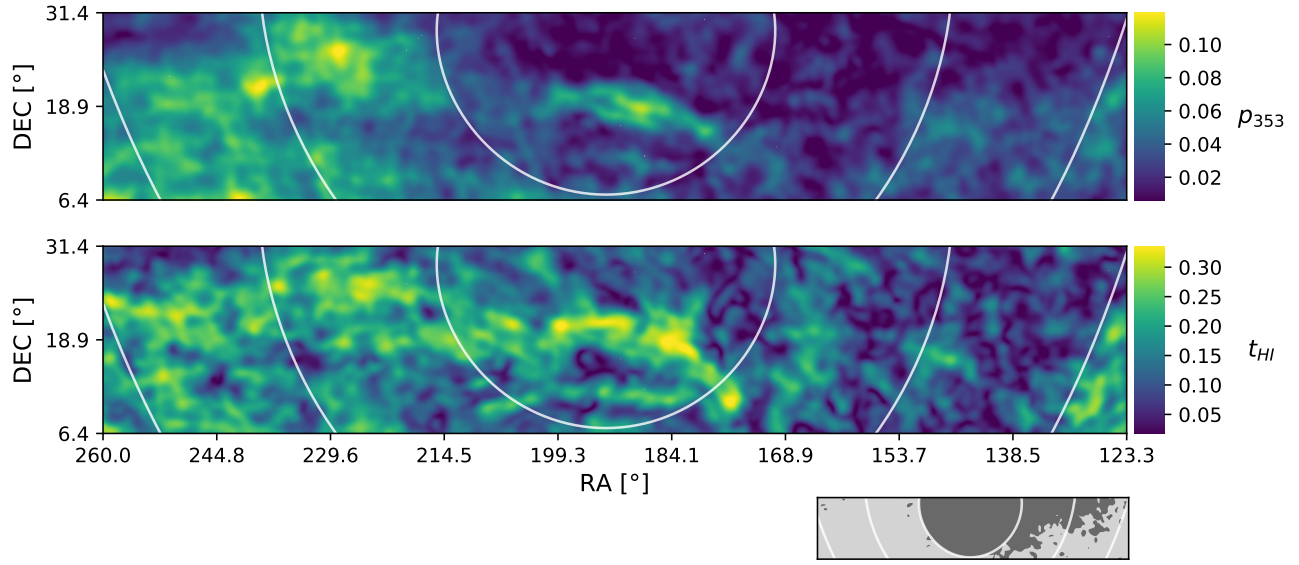


Figure 1. Sky maps of the *Planck* 353 GHz polarization fraction (top) and HI coherence (bottom). Note the different ranges on the color bars, which linearly map the 5-95% intensity range of their respective quantities. Both p_{353} and t_{HI} are shown at an angular resolution of $90'$. White lines are lines of constant Galactic latitude: $b = 30^\circ, 50^\circ, 70^\circ$, from left to center. The small inset shows the same region of sky, where regions in dark gray are masked from the analysis in Figures 2 and 3.

where ρ is the local dust density, θ is the plane-of-sky magnetic field orientation, γ is the angle between the line of sight and the local magnetic field, and s is distance (e.g., Wardle & Königl 1990). The construction of t_{HI} thus mimics this model, with local HI intensity replacing local dust intensity, θ_{RHT} replacing the plane-of-sky magnetic field orientation, and v_{lsr} replacing distance. Missing from the t_{HI} construction, however, is information about the relative orientation between the line of sight and the local magnetic field orientation (the $\cos^2\gamma$ term). Loosening this implicit assumption that the magnetic fields contain a negligible line-of-sight component would lower the values of t_{HI} . Incorporating a model of $\cos^2\gamma$ into a t_{HI} -like quantity might reduce some of the scatter in the $t_{HI} - p_{353}$ relationship; alternatively, t_{HI} and p_{353} could be used to fit an estimate of γ .

Figure 2 shows a two-dimensional histogram of p_{353} and t_{HI} for the subset of the data indicated in the inset of in Figure 1. We consider the data in Figure 1 below a Galactic latitude of $b = 70^\circ$, to avoid latitudes near Galactic zenith where uncertainties in the *Planck* data are high and contamination from the cosmic infrared background may be significant (Planck Collaboration XIX 2015). In order to include only sightlines where an appreciable fraction of the total HI column has been analyzed, we compute the ratio of the GALFA-HI data integrated over $|v_{lsr}| \leq 36.4 \text{ km s}^{-1}$ to the data inte-

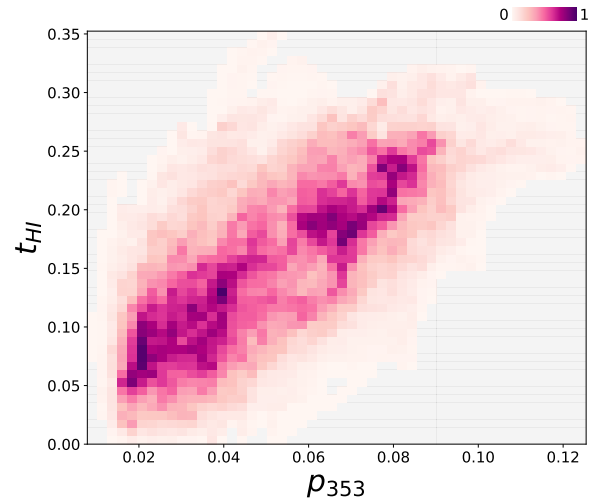


Figure 2. Two-dimensional histogram of the *Planck* 353 GHz polarization fraction (p_{353}) and HI coherence (t_{HI}). Colors represent the (normalized) pixel count value on a linear scale. Gray grid cells represent regions of the histogram with zero power. The region of sky analyzed is that in Figure 1, excluding pixels at Galactic latitudes $b > 70$ and pixels where the velocity range analyzed accounts for less than 90% of the $\pm 90 \text{ km s}^{-1}$ HI column, as discussed in the text.

grated over $|v_{lsr}| \leq 90 \text{ km s}^{-1}$ at $90'$ resolution. We mask pixels where this ratio is less than 0.9, though results are not strongly sensitive to this choice of ratio. For

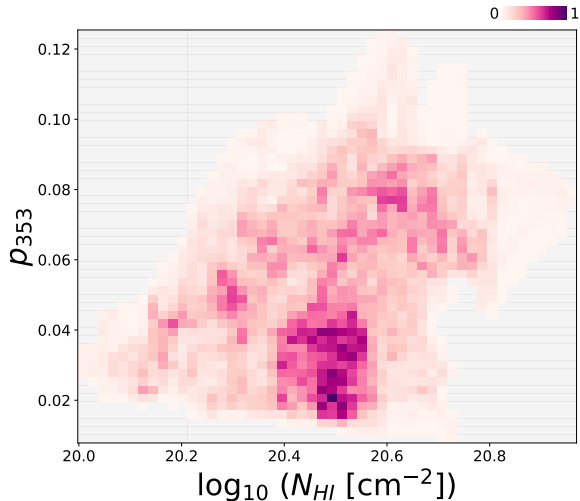


Figure 3. As in Figure 2, but for p_{353} and \log_{10} of the stray radiation-corrected GALFA-HI column density integrated over ± 90 km s $^{-1}$. The region of sky analyzed is the same as in Figure 2, and quantities are compared at FWHM=90'.

the masked pixels, more than 10% of the total HI column apparently lies at velocities outside of the range analyzed with the RHT. The individual velocity channel maps in the GALFA-HI data are not corrected for stray radiation, and so there also exist pixels where this ratio is greater than unity, due to noise. We retain these pixels but note that their removal does not qualitatively change Figure 2. Figure 2 shows a clear correlation between p_{353} and t_{HI} . A simple linear least-squares fit to this data yields $t_{HI} = 2.1p_{353} + 0.049$, with a correlation coefficient $r \sim 0.7$.

The corresponding two-dimensional histogram between $\log_{10}N_{HI}$ and p_{353} is shown in Figure 3. In this low column density ($< 10^{21}$ cm $^{-2}$) region there is no indication of the anticorrelation between N_H and p_{353} found at higher column densities (Planck Collaboration XIX 2015), and in fact this region displays a weak but significant positive correlation, with a linear correlation coefficient $r \sim 0.4$. These results do not depend strongly on the cuts made to the data. To estimate the robustness of these correlations we performed a block bootstrap analysis by dividing the sky into $100' \times 100'$ regions, sampling these regions with replacement 10^4 times, and fitting each sample with a least-squares linear regression. We find a 95% confidence interval for r of [0.65, 0.71] for the p_{353} - t_{HI} relation and [0.33, 0.41] for the N_{HI} - p_{353} relation. We conclude that HI coherence is positively correlated with p_{353} in low column regions where N_{HI} is not as strongly predictive of p_{353} .

4. DISCUSSION

This work extends our understanding of the link between neutral hydrogen morphology and the interstellar magnetic field. We establish for the first time that the velocity-space variation of HI orientation is a probe of line-of-sight magnetic field tangling. This is important both for our understanding of the magnetized interstellar medium and potentially for measurements of the polarized foreground to cosmology experiments.

The polarized dust emission at high Galactic latitudes is variable on the plane of the sky. Planck Collaboration XIX (2015) found that spatial variation in the fractional dust polarization at 353 GHz is anti-correlated with variation in the polarization angle dispersion – that is, regions with low fractional polarization correspond to regions where the projected polarization angle varies rapidly on the plane of the sky. This suggests that depolarization of the integrated dust emission is primarily caused by disordered magnetic fields on scales smaller than the polarization angle dispersion is measured ($\sim 1^\circ$). It seems likely that magnetic field tangling is primarily responsible for the spatial variation of p_{353} , rather than, for example, variable grain alignment efficiency (see also Planck Collaboration XX 2015). The present work supports this conclusion by demonstrating that p_{353} is correlated with the frequency-space variation in HI orientation, a quantity derived from data (HI) that is independent of the physics of grain alignment. This finding is consistent with expectations from grain alignment theory (e.g., Lazarian 2007).

Polarized dust emission is affected by physics at a range of scales, including the Galactic magnetic field structure and turbulence in the diffuse ISM, as well as dust grain population and alignment properties. A phenomenological model of polarized dust emission as the sum of N independent dust layers was shown to reproduce the one-point statistics of p_{353} and θ_{353} over the southern Galactic cap when $N \sim 4 - 9$ (Planck Collaboration XLIV 2016). The authors fit a single mean magnetic field orientation and assume the turbulent component of the Galactic magnetic field to be Gaussian and isotropic. This approach was expanded to include constraints from the Planck 353 GHz EE , BB , and TE power spectra by Vansyngel et al. (2017). These approaches, while not entirely physical, provide useful prescriptions for generating statistically representative, independent realizations of the polarized sky. By using power spectra constraints, Vansyngel et al. (2017) effectively introduced the observed correlation between density structures and the ambient magnetic field, which creates a TE correlation and a non-unity EE/BB ratio (Clark et al. 2015; Planck Collaboration XXXVIII

2016). In the Ghosh et al. (2017) model, this correlation is introduced by a single polarization layer in which the plane-of-sky magnetic field is perfectly aligned with HI structures associated with the cold neutral medium.

The work presented in this Letter suggests that new models can be constructed in which HI binned into velocity intervals serve as separate “layers,” each with HI structure orientation and HI intensity providing a template for the local magnetic field orientation and local dust intensity, respectively. This is a data-driven way to incorporate the anisotropy of magnetized turbulence, which is missing from the Planck Collaboration XLIV (2016) approach but a relevant astrophysical constraint (e.g., Brandenburg & Lazarian 2013). Indeed, magnetohydrodynamic turbulence predicts that elongated eddies rotate perpendicular to the local magnetic field, in agreement with the observation that structures in thin HI velocity channels are elongated in the direction of the field (Clark et al. 2014; Lazarian & Yuen 2018). The HI velocity layer approach outlined here would allow dust emission prescriptions to be mapped onto physical spatial variation, thereby complementing purely frequency-space dust models (e.g., Hensley & Bull 2018).

Modeling the polarized dust emission at high Galactic latitude is crucial for characterizing the polarized foreground to the CMB. Because the polarized dust emission peaks at frequencies much higher than the peak CMB emission, current foreground dust subtraction techniques use sky measurements at dust-dominated frequencies extrapolated to CMB-dominated frequencies of interest. This extrapolation implicitly assumes that the temperature of dust-emitting regions is uniform along the line of sight. If instead multiple regions (clouds) at different distances along the line of sight have different temperatures, they will each contribute differently to the emission at a given frequency. Measured Stokes parameters will change with frequency as clouds with different polarization properties contribute according to their SEDs. In particular, clouds along the line of sight that experience differently oriented magnetic fields – thus producing emission that is linearly polarized at different angles – will significantly decorrelate the polarized dust signal between ~ 350 and ~ 150 GHz (Tassis & Pavlidou 2015; Poh & Dodelson 2017).

If regions of significant misalignment of the magnetic field along the line of sight can be identified, they can be excluded from a CMB polarization analysis. One probe of the degree of magnetic field misalignment along the line of sight requires optical starlight polarization measurements at a number of different distances within a single CMB experiment beam (Tassis & Pavlidou 2015).

The synthesis of *Gaia* (Gaia Collaboration 2016) data for stellar distances and the planned PASIPHAE¹ experiment to measure polarization toward millions of high Galactic latitude stars will enable this sort of magnetic tomography.

For estimating the frequency decorrelation of polarized dust CMB foregrounds, however, it is necessary to know only what lines of sight harbor significantly misaligned magnetic fields, and not *where* in distance the different magnetic fields lie. Thus, this work demonstrates that the local intensity and orientation of linear HI features in different frequency intervals can identify regions with potentially problematic line-of-sight magnetic field tangling. Masks can be constructed from maps of t_{HI} or a similar metric. Additionally, HI morphology and the HI brightness in different line-of-sight velocity channels can be combined with dust SED prescriptions to model the polarized foreground as discussed above, and used to estimate the expected frequency decorrelation. This work utilizes HI data in the velocity range $|v_{lsr}| \leq 36.4$ km s⁻¹. We note that a wider velocity range may be necessary for lines of sight that intercept high-velocity clouds in the Galactic halo, some of which may contain detectable dust emission (Miville-Deschênes et al. 2005; Peek et al. 2009).

The large-scale structure of the Galactic magnetic field is a major open question, complicated by the fact that various observational probes trace different components of the magnetic field, in different phases of the ISM. The synthesis of multiwavelength data is therefore necessary to understand both the overall structure of the magnetic field and its distribution between ISM phases. Studies of the magnetic field often distinguish between components of the field, characterized by their isotropy in direction and strength, that originate from different physical processes (dynamoes, turbulence, etc.) and contribute differently to observables like the total and polarized synchrotron intensity and the Faraday rotation measure (RM; e.g., Jaffe et al. 2010). The relative dominance of these magnetic field components likely changes with ISM environment: recent multiwavelength work on the Galactic plane suggests that the Galactic magnetic field may be more ordered in dust-emitting regions than the average field traced by synchrotron and RM data (Jaffe et al. 2013). Additional constraints from the velocity coherence of HI orientation may be useful for disentangling the various components of the Galactic magnetic field in different ISM phases.

¹ <http://pasiphae.science>

This work illustrates a promising avenue for magnetic tomography with HI. If HI can be mapped to three dimensions, this will constitute an independent, local probe of the magnetic field orientation. This plane-of-sky information is complementary to tracers of the line-of-sight component of the magnetic field. In particular, the synthesis of Faraday tomography (Burn 1966; Brentjens & de Bruyn 2005) and three-dimensional dust maps (e.g., Lallement et al. 2014; Green et al. 2015) has recently shown promise for modeling the line-of-sight magnetic field in a small region of the nearby ($\lesssim 500$ pc) ISM (Van Eck et al. 2017). Future work incorporating both neutral and magneto-ionic data has the potential to constrain the three-dimensional magnetic field vector in three spatial dimensions in the ISM.

S.E.C. would like to thank the PSI2 program of the Université Paris-Saclay for support and hospitality during the program *The ISM Beyond Three Dimensions* when work on this paper was undertaken. We thank ISM3D organizers Marc-Antoine Miville-Deschênes and Josh Peek, and many other attendees for stimulating conversation, especially Vincent Guillet, François

Boulanger, Naomi McClure-Griffiths, and Alex Hill. We also thank J. Colin Hill, Yong Zheng, Brandon Hensley, and Mary Putman for useful discussions, and the anonymous referee for thoughtful feedback. We thank Ludovic Montier for the code used to smooth noise covariance matrices. S.E.C. is supported by NASA through Hubble Fellowship grant #HST-HF2-51389.001-A awarded by the Space Telescope Science Institute, which is operated by the Association of Universities for Research in Astronomy, Inc., for NASA, under contract NAS5-26555.

This publication utilizes data from Galactic ALFA HI (GALFA-HI) survey data set obtained with the Arecibo L-band Feed Array (ALFA) on the Arecibo 305m telescope. The Arecibo Observatory is operated by SRI International under a cooperative agreement with the National Science Foundation (AST-1100968), and in alliance with Ana G. Méndez-Universidad Metropolitana, and the Universities Space Research Association. The GALFA-HI surveys have been funded by the NSF through grants to Columbia University, the University of Wisconsin, and the University of California.

REFERENCES

- Beck, R., Brandenburg, A., Moss, D., Shukurov, A., Sokoloff, D. 1996, *ARA&A*, 34, 155
- BICEP2/Keck Collaboration & Planck Collaboration. 2015, *PhRvL*, 114, 101301
- Brandenburg, A. & Lazarian, A. 2013, *SSRv*, 178, 163
- Brentjens, M.A. & de Bruyn, A.G. 2005, *A&A*, 441, 1217
- Burn, B.J. 1966, *MNRAS*, 133, 67
- Chandrasekhar, S. & Fermi, E. 1953, *ApJ*, 118, 113
- Clark, S.E., Peek, J.E.G., Putman, M.E. 2014, *ApJ*789, 82
- Clark, S.E., Hill, J. C., Peek, J.E.G., Putman, M.E., & Babler, B.L. 2015, *PhRvL*, 115, 241302
- Ferrière, K. 2001, *Rev. Mod. Phys.*, 73, 1031
- Flauger, R., Hill, J.C., Spergel, D.N. 2014, *JCAP*, 8, 39
- Gaia Collaboration. 2016, *A&A*, 595, 2
- Ghosh, T., Boulanger, F., Martin, P. G., Bracco, A., Vansyngel, F., Aumont, J., Bock, J. J., Doré, O., Haud, U., Kalberla, P. M. W., Serra, P. 2017, *A&A*, 601, A71
- Green, G. M., Schlafly, E. F., Finkbeiner, D. P., Rix, H.-W., Martin, N., Burgett, W., Draper, P.W., Flewelling, H., Hodapp, K., Kaiser, N., Kudritzki, R.P., Magnier, E., Metcalfe, N., Price, P., Tonry, J., Wainscoat, R. 2015, *ApJ*, 810, 25
- Haverkorn, M. 2015, In: Lazarian A., de Gouveia Dal Pino E., Melioli C. (eds) *Magnetic Fields in Diffuse Media*. Astrophysics and Space Science Library, vol 407. Springer, Berlin, Heidelberg
- Hensley, B. & Bull, P. 2018, *ApJ*, 853, 127
- Jaffe, T.R., Leahy, J.P., Banday, A.J., Leach, S.M., Lowe, S.R., Wilkinson, A. 2010, *MNRAS*, 401, 1013
- Jaffe, T. R., Ferrière, K. M., Banday, A. J., Strong, A. W., Orlando, E., Macías-Pérez, J. F., Fauvet, L., Combet, C., Falgarone, E. 2013, *MNRAS*, 431, 683
- Jansson, R. & Farrar, G.R. 2012, *ApJ*, 757, 14
- Kalberla, P.M.W., Kerp, J., Haud, U., Winkel, B., Ben Bekhti, N., Flöer, L., Lenz, D. 2016, *ApJ*, 821, 117
- Lallement, R., Vergely, J.-L., Valette, B., Puspitarini, L., Eyer, L., & Casagrande, L. 2014, *A&A*, 561, A91
- Lazarian, A. 2007, *JQSRT*, 106, 225
- Lazarian, A. & Yuen, K. H. 2018, *ApJ*, 853, 96
- Miville-Deschênes, M.-A., Boulanger, F., Reach, W. T., Noriega-Crespo, A. 2005, *ApJL*, 631, 57
- Montier, L., Plaszczyński, S., Levrier, F., Tristram, M., Alina, D., Ristorcelli, I., Bernard, J.-P. 2015, *A&A*, 574, A135
- Montier, L., Plaszczyński, S., Levrier, F., Tristram, M., Alina, D., Ristorcelli, I., Bernard, J.-P. Guillet, V. 2015, *A&A*, 574, A136

- Peek, J.E.G., Heiles, C., Putman, M.E., Douglas, K. 2009, *ApJ*, 692, 827
- Peek, J.E.G., Babler, B.L., Zheng, Y., Clark, S.E., Douglas, K.A., Korpela, E.J., Putman, M.E., Stanimirović, S., Gibson, S.J., Heiles, C. 2018, *ApJS*, 234, 1
- Planck Collaboration. 2015, *A&A*, 576, 104
- Planck Collaboration. 2015, *A&A*, 576, 105
- Planck Collaboration. 2016, *A&A*, 594, 8
- Planck Collaboration. 2016, *A&A*, 586, 141
- Planck Collaboration. 2016, *A&A*, 596, 105
- Planck Collaboration. 2017, *A&A*, 599, 51
- Planck Collaboration. 2018, ArXiv e-prints, arXiv:1801.04945
- Plaszczynski, S., Montier, L., Levrier, F., Tristram, M. 2014, *MNRAS*, 439, 4048
- Poh, J. & Dodelson, S. 2017, *PhRvD*, 95,103511
- Seljak, U. & Zaldarriaga, M. 1997, *PhRvL*78, 2054
- Sheehy, C., & Slosar, A. 2018, *PhRvD*, 97, 043522
- Tassis, K., & Pavlidou, V. 2015, *MNRAS*, 451, L90
- Van Eck, C.L., Haverkorn, M., Alves, M.I.R., Beck, R., de Bruyn, A.G., Enßlin, T., Farnes, J. S., Ferrière, K., Heald, G., Horellou, C., Horneffer, A., Iacobelli, M., Jelić, V., Mart-Vidal, I., Mulcahy, D.D., Reich, W., Röttgering, H.J A., Scaife, A.M.M., Schnitzeler, D. H.F.M., Sobey, C., Sridhar, S.S. 2017, *A&A*, 597, 98
- Vansyngel, F., Boulanger, F., Ghosh, T., Wandelt, B., Aumont, J., Bracco, A., Levrier, F., Martin, P. G., Montier, L. 2017, *A&A*, 603, 62
- Wardle, M., & Königl, A. 1990, *ApJ*, 362, 120